SOILS AND FOUNDATIONS Vol. 47, No. 1, 11–25, Feb. 2007
Japanese Geotechnical Society

A THERMO-PORO-VISCO-PLASTIC SHEAR BAND MODEL FOR SEISMIC TRIGGERING AND EVOLUTION OF CATASTROPHIC LANDSLIDES

NIKOS GEROLYMOS[i], IOANNIS VARDOULAKIS[ii] and GEORGE GAZETAS[iii]

ABSTRACT

The goal of this paper is to develop a constitutive model for the rapid deformation of clay-rich shear zones. Such a model would be necessary to describe the seismic triggering and evolution of catastrophic landslides. The model is based on: (a) the well-documented in the literature strain-softening and viscoplastic behaviour of saturated clays, and (b) the concept of frictional softening due to heat generated pore-water pressures. The inelastic stress-strain relationship is described with a 1-dimensional cyclic constitutive model of the (Bouc-Wen) type, coupled with a Cam-Clay frictional law with hardening and a set of equations that govern the mechanism of heat-generated pore-water pressure build up. Calibration of the model parameters is accomplished through laboratory tests, with the help of artificial neural network analysis. The influence of key variables on the behaviour of a rapidly deforming shear band is thoroughly investigated and the results of the analysis are critically discussed.

Key words: catastrophic landslide, clay, heat generated pore-water pressures, neural network, shear band, thermo-plasticity, thermo-poro-viscoplasticity (**IGC**: B3/E8/E14)

INTRODUCTION

Dynamic deformation of a saturated clay-rich shear band involves strongly coupled material nonlinearities, such as: (a) strain softening (*slow* residual strength), (b) strain-rate dependency (*fast* residual strength), (c) thermo-viscoplastic softening due to heat-generated pore-water pressures, and (d) hysteretic stress-strain behaviour.

Numerous experimental results in the literature show the relationship with the aforementioned mechanisms of several index properties of a clayey soil (e.g., the fraction of platy particles, clay mineralogy, pore water chemistry, coefficient of interparticle friction, overconsolidation ratio, mean normal effective stress, fraction of rotund particles, existence of particle orientation, etc).

The residual strength of soil at slow drained shearing rates has been studied extensively during the last four decades. Various correlations between slow residual strength and index properties have been proposed (e.g. Lupini et al., 1981; Bishop et al., 1971; Skempton, 1985; Bromhead and Curtis, 1983; Tika and Hutchinson, 1999). Lupini et al. (1981) utilised the results of a large number of ring shear tests on natural soils to study the controlling mechanisms of residual shearing. They pointed out that three modes reflect the quantity of platy particles present in the soil:

(a) A turbulent mode, in soils with high fraction of rotund particles (i.e., with clay fraction lower than 20–25%), or with platy particles of high interparticle friction. The slow residual friction angle (the shear strength at slow displacement rates) is high and depends mainly on the shape and packing of the rotund particles, rather than the clay mineralogy (kaolinite, illite, montmorillonite, etc).

(b) A sliding mode, in soils with high platy clay (less than 2 μm) fraction generally larger than 40%–50%. A low-strength shear band of preferred platy particle orientation develops. Slow residual strength is mainly controlled by the interparticle friction of clay minerals, clay mineralogy, pore water chemistry, and normal effective stress. Skempton (1985) suggested the following typical values for representative clay minerals: 15° for kaolinite, 10° for illite or clay mica, and 5° for montmorillonite.

(c) A transitional mode, in which there is no dominant particle shape (platy or rotund), with clay fraction between 20% and 50%. Shearing involves both turbulent and sliding behaviour at different locations of the shear zone. In this mode, slow residual strength is sensitive to small changes in soil gradation.

[i] Post-Doctoral Research Civil Engineer, National Technical University of Athens, Greece (gerolymos@mycosmos.gr).
[ii] Professor of Applied Sciences, ditto.
[iii] Professor of Civil Engineering, ditto (gazetas@ath.forthnet.gr).
The manuscript for this paper was received for review on July 7, 2005; approved on July 26, 2006.
Written discussions on this paper should be submitted before September 1, 2007 to the Japanese Geotechnical Society, 4-38-2, Sengoku, Bunkyo-ku, Tokyo 112-0011, Japan. Upon request the closing date may be extended one month.

The influence of pore water chemistry upon the residual strength of pure and natural clays, exhibiting the sliding shear mode, has been studied by several researchers (e.g., Moore, 1991; Anson and Hawkins, 1998). They demonstrated that the type and concentration of cations in the pore water significantly affects the residual shear strength. Moore (1991), exploiting the results of a series of ring shear tests on saturated clays, showed that alteration in residual shear strength (caused by the presence of exchangeable cations in pore water) increases with increasing specific surface area of clay particles. He reported an average increase of the residual friction angle of about 2°, for a calcium-exchanged kaolinite compared with a sodium-exchanged kaolinite. The increase is larger, reaching 5°, when the predominant clay mineral is montmorillonite. Salt concentration was also found to influence the residual strength. An increase, of about 1° to 2° in the residual friction angle of London and Weald Clay (with illite the predominant mineral), respectively, was reported by Moore (1991).

Although numerous studies have been carried out regarding the residual strength of clayey soils tested in the ring shear apparatus, only a few of them were dedicated to the fast residual strength, i.e., the ultimate strength at fast displacement rates. Tika et al. (1996) studied the fast shearing response of pre-existing shear zones and presented results for a wide range of natural soils. According to their research, three types of rate effect on the residual strength are identified:

(a) A positive rate effect, in soils showing a fast residual strength higher than the slow one. This type of viscous behaviour is associated only with the sliding shear mode.

(b) A negative rate effect, in soils showing a significant drop of fast residual strength below the slow residual strength, when sheared at rates higher than a critical value. Soils with transitional or sliding shear mode may exhibit this type of behaviour. In some tests, fast residual strength was measured to be as low as 60% of the slow residual strength.

(c) A neutral rate effect, in soils showing a fast residual strength nearly equal to the slow residual irrespective of displacement rate, associated with the turbulent shear mode.

Tika et al. (1996) clarified that: (a) the fast residual strength is reached when the displacement rate surpasses a critical value; (b) strength is slightly affected by excess pore water pressure arising from the contractive behaviour or from heating of the clay, and (c) the negative effect on residual strength results from the increased soil flow potential due to water absorption by the shear band, caused by its dilative behaviour.

However, the critical velocity required to reach the fast residual strength was measured to be in the order of 0.005 m/s to 0.1 m/s. This is far smaller than the one required for initiation of heat generated pore water pressures, which can be of the order of few meters per second for overconsolidated clays (Vardoulakis, 2002). On the other hand, it has been proven by several researchers that large

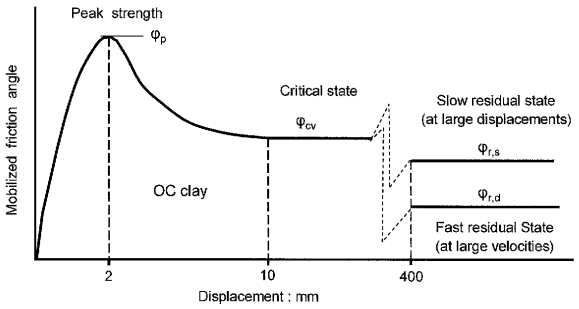

Fig. 1. Idealized evolution of the mobilized friction angle during the sliding process in a ring shear apparatus

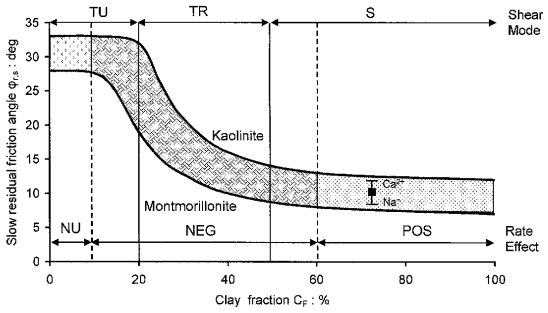

Fig. 2. Diagrammatic correlation of slow residual friction angle with the clay fraction: The three regions of different shear mode behaviour (TU, TR, S) and the three regions of different consequences (neutral, negative, positive) of the rate of shearing on residual strength, are: The error band of the single experimental point represents the effect of pore water chemistry on residual strength

(even enormous) velocities are developed in catastrophic landslides. For example, referring to the disastrous Vaiont slide, back-analysis indicated that the sliding mass moved some 400 m, reaching a maximum velocity of 20 to 40 m/s (Mench, 1966; Habid, 1967, 1976; Goguel, 1978; Muller, 1964, 1968; Ciabatti, 1964; Voight and Faust, 1982; Vardoulakis, 2002). It is thereby evident that thermo-poro-mechanical behaviour of clays is a critical issue in the evolution of catastrophic landslides. Nevertheless, it is pointed out that frictional strain-rate softening without heat-generated pore-water pressures may, under certain conditions, lead to accelerated creep (Vardoulakis, 2000). This means that frictional rate-softening behaviour is by itself a significant destabilizing factor.

The above conclusions on shear behaviour of clay are elucidated in Figs. 1 and 2.

It is well documented in the literature that clays are thermo-viscoplastic materials (Campanella and Michell, 1968; Nova, 1986; Hueckel and Baldi, 1990). Hicker (1974), Despax (1976), Modaressi (2002), and Laloui and Cekerevac (2003) reported that some clays demonstrate thermoplastic softening behaviour, referring to their friction coefficient in the critical state, while others are practically unaffected by temperature. Modaressi and Laloui (1997) pointed out that when a clay sample is heated slowly enough to allow complete draining, two phases of behaviour can be distinguished:

- a reversible phase, termed "thermoelasticity", due to dilation of the mineral components, and
- an irreversible phase, termed "thermoplasticity", caused by both dilation of clay minerals and collapse of the absorbed water, resulting in failure of some interparticle ties.

Experimental work identifies that the response of an overconsolidated (OC) clay in thermal loading is different from that of a normally (NC) to slightly overconsolidated clay. In an OC clay, thermoelastic dilation during the heating phase is followed by thermoelastic contraction during the cooling phase. In a NC clay, thermoplastic contraction during the heating phase is usually followed by additional thermoelastic contraction during the cooling phase. However, Sultan (1997), and Laloui and Cekerevac (2003) showed that at high temperatures, above a critical value, overconsolidated clays sustain thermoplastic contraction as well.

In drained loading conditions, thermoplastic contraction results in shear strength increase due to soil densification. Under undrained conditions, the natural trend of the soil for thermoplastic contraction gives rise to an increase in pore water pressure, which in turn results in frictional softening. On the other hand, thermoelastic dilation either would not affect at all or would only slightly increase the soil shear strength. The preconsolidation stress is also affected by temperature, being a decreasing function of it. Thus, under drained loading conditions as temperature increases the brittle and dilative behaviour of an overconsolidated clay alters to a more ductile and less dilative (or even contractive) behaviour.

Vardoulakis (2000) starting from a set of axiomatic principles, reformulated the equations that govern the motion of a rapidly and monotonically deforming shear band. The soil was considered as a two-phase mixture of solids and fluid, and the governing equations were derived from the corresponding conservation laws of mass, momentum and energy. The resulting governing equations are two coupled diffusion-generation partial differential equations, containing two unknown functions: excess pore-water pressure and temperature inside the shear band. The velocity field is considered as an external loading, and therefore is presumed known. He applied his model to analyse the Vaiont slide, having calibrated the model parameters on experimental data, from the literature. Strain and strain-rate induced frictional softening was also considered in the analysis by utilising results from ring shear tests on Vaiont clay specimens conducted by Tika and Hutchinson (1999).

In this paper the governing equations of heat-generated pore pressures inside a rapidly deforming shear band, are summarised. Their formulation is limited to adiabatic and undrained response conditions. Then a constitutive model is developed consisting of the aforementioned equations, coupled with: (i) a 1-dimensional Bouc-Wen type constitutive model (Gerolymos and Gazetas, 2005) for the hysteretic stress-strain behaviour of the shear band in cyclic loading, (ii) a Cam-Clay model with a hardening rule for the frictional behaviour of soil before the formation of the shear band (at the critical state), and (iii) a visco-plastic model for strain and strain-rate softening at large displacements (residual state).

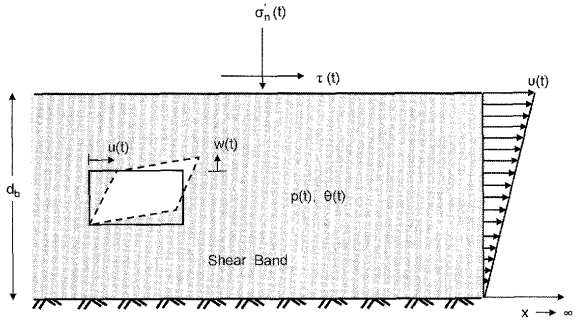

Fig. 3. Schematic illustration of the shear band model

A comprehensive methodology for calibration of the model parameters, is also presented by resorting to published experimental data. Closed-form expressions are developed from correlation of the key parameters with characteristic index soil properties, making use of artificial neural network analysis.

The objectives of the paper are (a) to develop a shear band model for the analysis of seismic triggering and evolution of catastrophic landslides, (b) to present a methodology for calibrating the model parameters when relevant experimental data is scarce, and (c) to perform a (limited) parametric analysis of a dynamically deforming shear band.

The proposed model aims at joining theoretically the initiation of a landslide due to seismic loading and the response of the slide at extremely large deformations. According to the authors' knowledge only a limited amount of studies is devoted to this issue, including the recent work of Chang et al. (2005).

CONSTITUTIVE MODEL: EQUATIONS AND PARAMETERS

Problem Definition

The problem studied is that of a deforming shear band consisting of saturated clay, subjected to shear loading. The shear band is considered of infinite length and of thickness d_b (Fig. 3). Both of its boundaries are assumed impermeable to fluid flow and nonconductive to heat flux. This means that the field variables in the shear band, namely excess pore water pressure p, temperature θ, and shear strain γ, are functions only of time t. Such boundary conditions imply undrained and adiabatic response, which is realistic when the shear band is deformed at large velocity, as it is generally the case in a catastrophic landslide. Excess pore water pressure and heat would not have the time to dissipate rapidly, especially when the thickness of the shear band is relatively large.

We assume the shear band thickness to be constant during the sliding process. It is noteworthy that the evolution of shear band thickness with displacement is not well documented in the literature (Otsuki, 1978;

Waterson, 1986; Drescher et al., 1990). It is assumed here that the shear band has been completely formed after the critical state of the soil has been reached. Hence, the plastic volumetric strain rate is assumed to be equal to zero (zero plastic dilatancy) and only shear strain is considered. The behaviour before shear band formation is modeled with a Cam-Clay frictional law (Modaressi et al., 1995). In that stage, volumetric strain rate is also considered. Eventually, the hysteretic stress-strain behaviour of the shear band is described with a Bouc-Wen type model such as the one presented by Gerolymos and Gazetas (2005).

Model for Frictional Behaviour

A versatile one-dimensional macroscopic model is utilized to describe the shear stress-strain relationship inside the shear band. The model is capable of reproducing an almost endless variety of stress-strain forms, monotonic as well as cyclic. Based on the original proposal by Bouc (1971) and Wen (1976), the model was extended by Gerolymos and Gazetas (2005) and applied to cyclic response of soils. A simple version of the model is briefly outlined here.

The shear stress τ at a particular time t is expressed as:

$$\tau(u(t)) = \tau_y(u(t))\zeta(u(t)) \tag{1}$$

where u is the lateral displacement (tangential to the sliding surface), τ_y is the ultimate shear strength of soil, and $\zeta = \zeta(u(t))$ is a dimensionless "hysteretic" parameter controlling the nonlinear response; it is expressed with the following differential equation:

$$\frac{d\zeta}{dt} = \frac{1}{u_y}\left[\frac{du}{dt} - \left(b\frac{du}{dt}|\zeta|^n + (1-b)\left|\frac{du}{dt}\right||\zeta|^{n-1}\zeta\right)\right] \tag{2}$$

in which: $\dot{u}$ is the lateral velocity; u_y is a parameter signaling the end of elastic slip (a rigid plastic behaviour is approximated by assuming a very small value of u_y, say less than $<10^{-3}$ m). n and b are dimensionless quantities that control the shape of the hysteresis loop. Equation (2) is obviously of a hysteretic rather than a viscous type. Hence, its solution is not frequency dependent. By eliminating t, it can be rewritten in an incremental $d\zeta$-du form:

$$\frac{d\zeta}{du} = \frac{1}{u_y}\{1 - |\zeta|^n[b + (1-b)\,sign\,(\dot{u}\zeta)]\} \tag{3}$$

By differentiating Eq. (1) with respect to the lateral displacement u:

$$\frac{d\tau}{du} = \tau_y\frac{d\zeta}{du} \tag{4}$$

and obviously that when ζ tends to 0, Eq. (3) reduces to:

$$\frac{d\zeta}{du} = \frac{1}{u_y} \tag{5}$$

Substituting Eq. (5) into Eq. (4) one obtains:

$$\left.\frac{d\tau}{du}\right|_{\zeta\to 0} = \frac{\tau_y}{u_y} \tag{6}$$

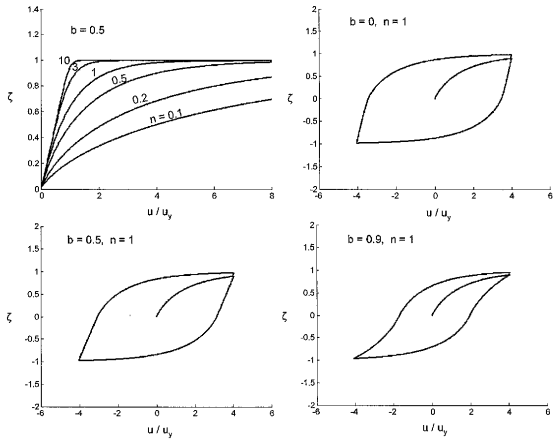

Fig. 4. ζ versus normalized displacement u/u_y curves for different values of parameter n for monotonic loading and different b values for unloading-reloading hysteresis loops

Equation (6) implies that the ratio τ_y/u_y is the initial stiffness of the shear band (in units of kN/m^3). From Eq. (1) it is obvious that the ultimate shear strength, τ_y, is reached when ζ tends to 1. For monotonic loading the maximum value of ζ is obtained by setting $d\zeta/du = 0$, and by virtue of Eq. (3) this maximum takes the value:

$$|\zeta_{max}| = 1 \tag{7}$$

From Eqs. (3) and (7) it is obvious that ζ takes values between -1 and 1.

Parameter n governs the sharpness of the transition from the linear to the nonlinear range, during initial virgin loading. It ranges from 0 to ∞, with elastic-perfectly-plastic behaviour practically achieved when n takes values greater than 10. Values of n between 0.6 and 1 have been found to better fit experimental results (Gerolymos and Gazetas, 2005). Parameter b controls the shape of unloading-reloading curve. Its range of values is between 0 and 1. When $b = 0.5$ the stiffness upon loading reversal equals the initial tangent stiffness, and the Masing criterion for loading-unloading-reloading arises. Monotonic loading curves for different values of n are presented in Fig. 4. Hysteresis loops of the parameter ζ versus the normalized displacement u/u_y for selected values of b are plotted in the same figure. For more details on Eq. (2) and calibration of the associated parameters, the reader is referred to the recent publication of Gerolymos and Gazetas (2005).

The shear strength τ_y is given by a Cam-Clay friction law with hardening rule (Modaressi et al., 1995), appropriately modified to be used in conjunction with the hysteretic Bouc-Wen model, and Terzaghi's effective stress principle:

$$\tau_y = \mu F \sigma'_n \tag{8}$$

in which μ is the mobilized friction coefficient, expressed in terms of Coulomb friction angle in direct shear:

$$\mu = \tan\varphi \tag{9}$$

and

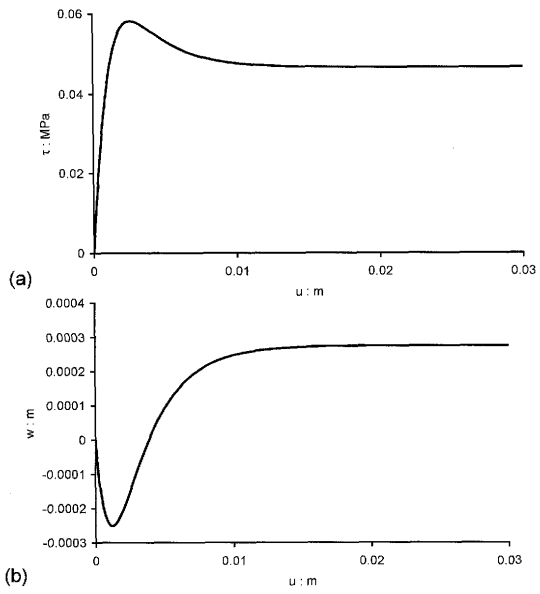

Fig. 5. (a) Shear force-tangential displacement and (b) normal versus tangential displacement, computed with the developed Bouc-Wen-Cam-Clay model (Model parameters: $n=1$, $b=0.5$, $k=0.2$, $\lambda=4000$, $\sigma'_{n0}=0.1$ MPa, $\sigma_{c0}=0.3$ MPa, and $\varphi=25°$)

$$\sigma'_n=\sigma'_{n0}(1-r_u),\quad r_u=\frac{p}{\sigma'_{n0}} \tag{10}$$

where σ'_{n0} is the initial effective stress normal to the shear band, and r_u the ratio of excess pore water pressure p normalized to σ'_{n0}. The term F in Eq. (8) is introduced to prevent the irreversible volumetric strain from increasing unlimitedly on a dilatant sliding surface. It is expressed as:

$$F=1-k\ln\left(\frac{\sigma'_n}{\sigma_c}\right) \tag{11}$$

with

$$\sigma_c=\sigma_{c0}e^{-\lambda w} \tag{12}$$

where w is the vertical displacement (normal to sliding surface), k is a shape parameter, and λ is the volumetric hardening parameter. σ_{c0} is the initial critical pressure which is by definition one-half of the preconsolidation stress. The evolution of vertical displacement is described by the following dilatancy rule proposed by Modaressi (1995):

$$dw=\left(-\tan\psi+\frac{|\tau|}{\sigma'_n}\right)|du| \tag{13}$$

in which ψ is a parameter for dilatancy, taken equal to the mobilized friction angle φ in this study. Details on the calibration of the Cam-Clay model parameters can be found on the work of Modaressi (1995).

As an example, Fig. 5 illustrates curves of shear stress and normal displacement versus tangential displacement for an overconsolidated clay subjected to monotonic shear loading, as computed with the proposed Bouc-Wen-Cam-Clay model. Notice, that when the shear band is being formed, at approximately $u\approx 0.01$ m, the rate of vertical displacement is practically becoming equal to zero.

As described in the introduction, the mobilized friction coefficient μ is a function of both displacement and velocity. It can be approximated by the following set of equations:

$$\mu=\min\{\min[\bar{\mu}(t<t_0)],\quad \bar{\mu}(t=t_0)\} \tag{14}$$

$$\frac{\bar{\mu}}{\mu_{cv}}=\frac{\mu_r}{\mu_{cv}}+\left(1-\frac{\mu_r}{\mu_{cv}}\right)e^{-\alpha u} \tag{15}$$

$$\frac{\mu_r}{\mu_{r,s}}=\frac{\mu_{r,d}}{\mu_{r,s}}+\left(1-\frac{\mu_{r,d}}{\mu_{r,s}}\right)e^{-\beta v} \tag{16}$$

where v $(=\dot{u})$ is the velocity, and μ_{cv}, μ_r, $\mu_{r,s}$ and $\mu_{r,d}$ are the critical state, residual, slow residual, and fast residual friction coefficients, respectively. The residual friction coefficient μ_r, varies between the two extremes: $\mu_{r,s}$ and $\mu_{r,d}$. The parameters α and β control the state of softening and of rate-softening/hardening of the frictional resistance, respectively. Equation (14) indicates that frictional softening is irreversible, so it is not recovering during cyclic sliding. In other words, the value of the mobilized friction coefficient μ is computed as the minimum between the value of $\bar{\mu}$ at current time step $(t=t_0)$ and the minimum value of $\bar{\mu}$ during the previous time steps $(t<t_0)$. The critical state coefficient μ_{cv} is defined for a possible state, in which shear is at constant volume but with random particle orientation, whereas the residual friction coefficient μ_r is defined for the state in which shearing takes place is at preferred particle orientation (Lupini et al., 1981).

The original Cam-Clay model is not valid after the critical state point (after the shear band has formed), whereas the proposed Bouc-Wen-Cam-Clay model is valid even for displacements larger than those required to reach the residual state of the soil. Furthermore, drained soil behaviour is assumed before the formation of the shear band. This is true under the assumption that pore water pressures are generated only due to temperature rise. As it will be shown in the sequence, heat generated pore water pressures are associated with large displacements which are usually of the order of 1m.

Calibration of the aforementioned parameters should be achieved through laboratory tests (e.g. ring shear). However, a methodology is presented herein for relating those parameters to key index soil properties or stress variables (e.g. clay fraction, plasticity index, effective normal stress, etc.).

Equations for Heat Generated Pore Pressure

Starting from the principles of mass and energy conservation in a two-phase soil element, Vardoulakis (2000) re-formulated a set of two coupled equations that govern the mechanism of heat generated excess pore-water pressure. In the limiting case of undrained shear response, the equation of pore water pressure generation is:

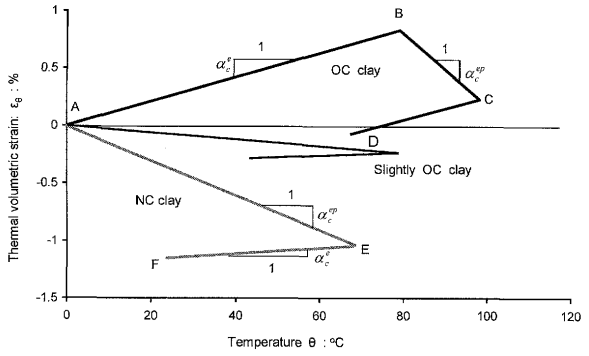

Fig. 6. Idealized isotropic thermal volumetric deformation of a normally consolidated (NC), a slightly overconsolidated and a heavily overconsolidated (OC) clay: The following branches are identified: OC Clay: (i) Heating phase: A-B, thermoelastic expansion: B-C, thermoplastic contraction and (ii) cooling phase: C-D, thermoelastic contraction: NC clay: (i) Heating phase: A-E, thermoplastic contraction and (ii) cooling phase: E-F, thermoelastic contraction

$$\frac{dp}{dt}=\lambda_m\frac{d\theta}{dt} \tag{17}$$

in which λ_m is the pore-pressure-temperature coefficient (in units of stress per temperature) given by the following two-branched expression:

$$\lambda_m=\begin{cases}0, & \theta\le\theta_{cr}\\ \dfrac{\alpha_c^{e}-\alpha_c^{ep}}{c}, & \theta\ge\theta_{cr}\end{cases} \tag{18}$$

where α_c^{e} and α_c^{ep} are illustrated in Fig. 6 and c is given in Eq. (19) below. In this limit the shear band boundaries are pressure-shock surfaces and it is meaningful to assume that the excess pore-water pressure p is uniformly distributed along the thickness of the shear band. In other words p is only a function of time.

As illustrated in Fig. 6, the thermal volumetric strain in a drained heating test under constant isotropic stress, may be expressed as a bilinear function of temperature. Since preconsolidation stress is also a function of temperature, the bilinear behavior is only an approximation. α_c^{e} is the slope of the volumetric thermal strain-temperature ($\varepsilon_\theta-\theta$) curve, associated with thermoelastic expansion in overconsolidated clay and with thermoelastic contraction in normally to slightly overconsolidated clay. Similarly, α_c^{ep} is associated with thermoplastic contraction in both overconsolidated and normally consolidated clay.

The parameter c in Eq. (18) is the oedometric compressibility of the water-saturated drained soil, approximated (after some algebra) by:

$$c=\frac{2}{3}(1+\nu)\frac{1}{1+e_0}\frac{C_r}{\sigma'_{n0}\ln(10)} \tag{19}$$

where ν is the Poisson's ratio of the soil skeleton under fully drained conditions, e_o is the initial void ratio of the soil, and C_r is the re-compression index in a reloading cycle, assumed here for simplicity to be identical to the "swelling" index in a unloading cycle. Due to lack of any significant information on the dependence of the Poisson's ratio ν and of C_r on temperature, we (tentatively, at least) assume that they are both independent of temperature.

Notice in Eq. (18) that the coefficient λ_m is either null or positive, depending on whether the temperature surpasses a critical value θ_{cr}, and whether the clayey soil is behaving thermoelastically or is collapsing in a thermoplastic manner. We also note that Eq. (17) is not valid as soon as vaporization takes place. This happens when the temperature surpasses the critical value for vaporization, which is approximated by the solution of the following equation (Vardoulakis, 2002):

$$\sigma'_{n0}-(62\theta+16926)\exp\left(-\frac{4650}{\theta+273}\right)\approx 0 \tag{20}$$

In the limiting case of adiabatic loading conditions the temperature profile inside the shear band is considered to be uniform and only variation with time is assumed. In this case the governing equation of heat generation is:

$$\frac{d\theta}{dt}=\frac{1}{j(\rho C)_m}D \tag{21}$$

where j (=4.2 J/cal) is the mechanical equivalent of heat, and $(\rho C)_m$ represents the specific heat multiplied by the mass density of the soil-water mixture. Picard (1994) proposed that

$$j(\rho C)_m=2.85\ \text{MPa}/^\circ\text{C},$$

for water-saturated clays. D expresses the rate of mechanical work due to frictional heating of the soil inside the shear band. By neglecting all dissipation in the fluid, D coincides with the rate of work of the shear stress deforming the soil skeleton:

$$D=\tau_y\zeta\dot{\gamma} \tag{22}$$

in which $\dot{\gamma}$ is the rate of shear strain measured after the shear band formation. The shear strain γ is expressed as a function of lateral displacement u and shear band thickness d_b

$$\gamma=\frac{\langle u-u_{cv}\rangle}{d_b} \tag{23}$$

where u_{cv} is the lateral displacement at critical state (corresponding to zero rate of volumetric strain). The symbol $\langle\cdot\rangle$ in Eq. (23) are the Macaulay brackets: $\langle x\rangle=x$, *if* $x\ge 0$; $\langle x\rangle=0$, *otherwise*. Therefore, Eq. (21) is active only after the development of shear band.

EVOLUTION OF SHEARING RESISTANCE DURING SLIDING

As elucidated in Fig. 7, the sliding process can be divided into the following three phases.

(a) *Pre-shear-band behaviour*: The behaviour of the soil at first shearing should follow the path A-B-C in Fig. 7. The peak strength is mobilized at the very early stage of displacement, and then drops to the critical state, triggering the creation of shear band. Beyond this point, the volumetric displacement is

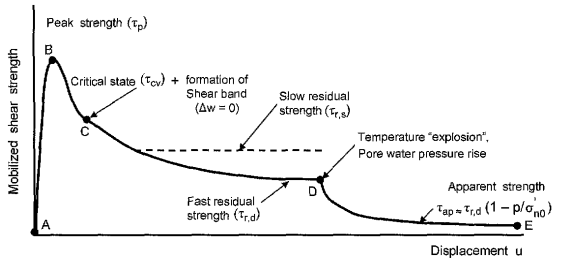

Fig. 7. Idealized evolution of the mobilized shear band resistance during the sliding process: The following phases are identified: *Pre-shear-band behaviour*: A-B-C, *Material softening*: C-D, and *Thermo-poro-mechanical softening*: D-E

assumed to vanish. The soil behaviour in this phase is governed by Eqs. (1), (2), and (13).

(b) *Material softening*: During this phase, the evolution of shearing resistance is depicted by path C-D. The material inside the shear band is frictionally softening due to strain and strain rate increase (if the material exhibits negative rate effect). This frictional softening is accompanied by temperature rise. The soil behaviour in this phase is governed by Eqs. (1), (2), and (14).

(c) *Thermo-poro-mechanical softening*: This phase, corresponding to path D-E, starts as soon as the temperature inside the shear band surpasses a critical value. Beyond this critical point, heat generated pore water pressures develop, causing further frictional softening. Eventually a residual steady state condition is reached, because:
- excess pore water pressures cannot exceed the initial effective stress, σ'_{n0}, and
- heat generated pore water pressures diminish gradually due to frictional softening.

The mechanisms of this phase are governed by Eqs. (1), (2), (17), and (21).

Phases (a) and (b) are responsible for the landslide triggering, but they also influence its evolution. On the contrary, phase (c) affects only the landslide evolution; it is the major destabilizing factor that contributes to accelerated "creep" and may transform a slope instability to a catastrophic landslide.

CALIBRATION OF MODEL PARAMETERS

A methodology is presented for the calibration of the model parameters by utilising experimental data from the literature. The methodology is based on correlating with key index soil properties, by means of artificial neural networks.

Parameters of Frictional Strain Softening

A so-called "multilayer perceptron" (MLP) network for function approximation was developed to correlate the slow residual friction angle $\varphi_{r,s}$ with key index soil properties. The reader is referred to the MATLAB user's manual for details in neural network analysis (theory and terminology). The neural network, consisting of three

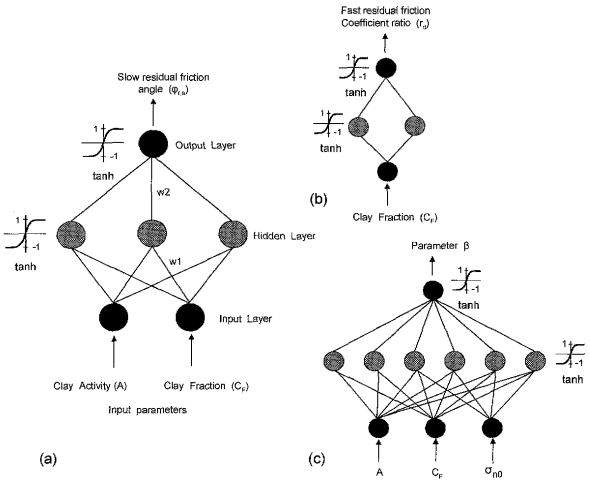

Fig. 8. Schematic illustration of multi-layer perceptron neural networks developed for correlation of the model parameters with key index soil properties: All three networks consist of three layers with the hyperbolic tangent as the transfer "activation" function of their neurons

layers, is schematically illustrated in Fig. 8. As shown in Fig. 8(a), the input layer comprises two input neurons ($m=2$) representing the following parameters (patterns):
- the clay fraction C_F, and
- the clay activity A

The latter is related to plasticity index I_p:

$$I_p = A C_F \tag{24}$$

The "hidden" layer of the network consists of three neurons ($h=3$) and the output layer of one neuron, representing the slow residual friction angle $\varphi_{r,s}$. The hyperbolic tangent function is used as the "activation" function of all neurons. *Training* of the neural network is achieved with repeated trials, using the mathematical computer code MATLAB. The input data base used for this training, consists of results from ring shear tests such as those of Tika et al. (1996) , Tika and Hutchinson (1999), Lupini et al. (1981), Skempton (1985), Bishop (1971), and Moore (1991).

The mathematical formulation of the neural network after the training, is expressed as:

$$\varphi_{r,s} = \tanh\left[\sum_{i=1}^{h} w2_i \tanh\left(\sum_{j=1}^{m} w1_{i,j}\bar{x}_j + b1_i\right) + b2\right] \tag{25}$$

where $w1_{i,j}$ and $b1_i$ are the weights and biases of the hidden layer, and $w2_i$ and b_2 the weights and biases of the output layer, given in Table 1. $\bar{x}_j$ is the normalized input vector with respect to the minimum values of the problem parameters x_j ($x_1 = A$, $x_2 = C_F$). $\bar{x}_j$ is expressed as a linear function of x_j according to:

$$\bar{x}_j = 2\frac{x_j - \min x_j}{\max x_j - \min x_j} - 1 \tag{26}$$

The (min, max) values of parameters x_j are (0.4, 4) and (0, 80) for A and C_F, respectively. The capability of the neural network model to "predict" the slow residual friction angle of the various experiments is demonstrated

Table 1. Weights and biases for the slow residual friction angle $\varphi_{r,s}$

Hidden layer			Output layer	
$w1_{i,j}$		$b1_i$	$w2_i$	$b2$
0.254	−0.068	1.555	−21.407	20.941
−0.208	0.747	0.713	−3.149	
−5.009	−3.78	−5.811	0.43	

Table 2. Typical displacements at various stages of shear in intact clays having $C_F > 30\%$ and at $\sigma'_{n0} < 600$ kPa (Skempton, 1985)

Stage	Displacement: mm	
	O-C	NC
Peak	0.5–3	3–6
Rate of volume change approximately zero	4–10	
At $\varphi_{r,s}+1°$	30–200	
Slow residual φ_r	100–500	

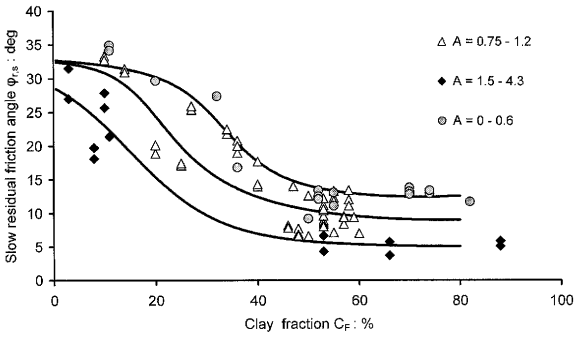

Fig. 9. Slow residual friction angle versus clay fraction and clay activity: Comparison between experimental data and the artificial neural network approximation: Data points taken from Tika et al., 1996; Tika and Hutchinson, 1999; Lupini et al., 1981; Skempton, 1985; Bishop et al., 1971 and Moore, 1991

in Fig. 9.

The subsequent task is to calibrate the parameter α of Eq. (15) that governs the transition from critical to slow residual state. Skempton (1985) proposed typical values of displacement at various stages of shear in intact clays; they are given in Table 2 and are valid for clay fractions higher than 30% and effective normal pressures σ'_{n0} lower than 600 kPa. These values are consistent with results from ring shear tests on sand-mica mixtures conducted by Lupini et al. (1981). Note that, the displacement required to reach the slow residual friction coefficient was 30 mm for soil specimens exhibiting turbulent shear mode, 100 mm for transitional shear mode, and 400 mm for sliding shear mode. Evidently, the magnitude of the effective normal stress σ'_{n0} and the presence of structural discontinuities also have a significant influence on the shear behaviour of clays. The reader is referred to the works of Skempton (1985) and Lupini et al. (1981). Figure 10 compares analytical [computed with Eq. (15)] versus laboratory (ring shear test) results for the Vaiont clay taken from Tika and Hutchinson (1999).

A neural network was also developed for a shear mode soil classification (Fig. 11). In this case the network

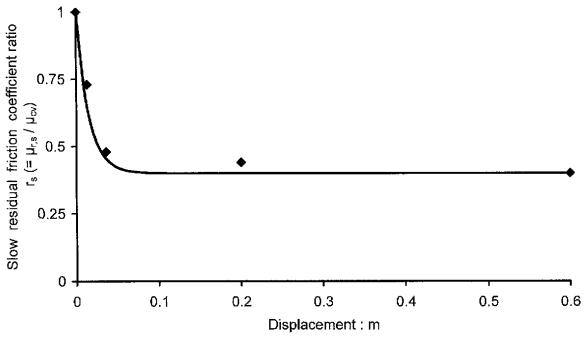

Fig. 10. Slow residual friction coefficient ratio (normalized with the friction coefficient μ_{cv} at critical void ratio) versus displacement: Comparison between measured in ring shear apparatus and computed behaviour, for $\alpha = 67$: The experimental points taken from Tika and Hutchinson, 1999, correspond to Vaiont clay with plasticity index $I_p = 22$, clay fraction $C_F = 30$, effective normal pressure $\sigma'_{n0} = 0.5$ MPa, and critical state friction coefficient $\mu_{cv} = 0.48$

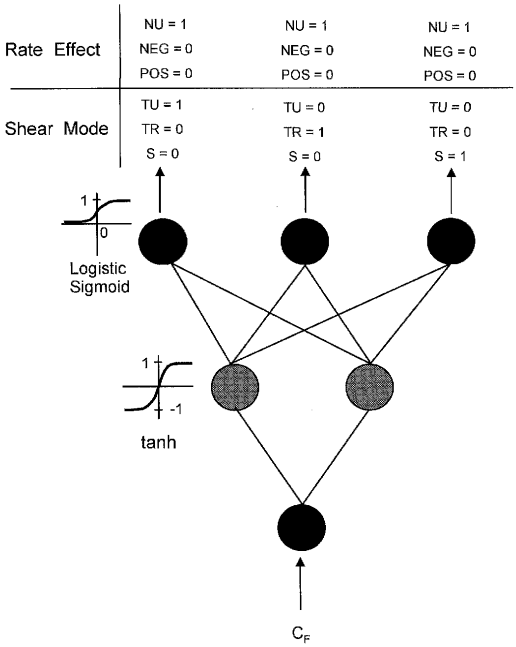

Fig. 11. Schematic illustration of multi-layer perceptron neural networks developed for classification of clays according to shear mode behaviour and rate effect on residual strength, in terms of the clay fraction: The networks consist of three layers with the hyperbolic tangent and logistic sigmoid as the transfer functions of the hidden and output neurons, respectively

consists of one input neuron representing the clay fraction C_F, two hidden neurons, and three output neurons, each corresponding to one of: turbulent mode (TU), transitional mode (TR), and sliding shear mode (S); "target" values are 1 for the correct class and 0 otherwise. The prediction of the neural network after training, is plotted in Fig. 12. Values between 0 and 1 represent the uncertainty of the network prediction. According to the results, the possibility of a clayey soil to exhibit turbulent shear mode is high for $C_F < 20\%$, low for $20\% < C_F < 40\%$, and zero for $C_F > 40\%$. In the same way, the possibility for transitional shear mode is low for $C_F < 20\%$,

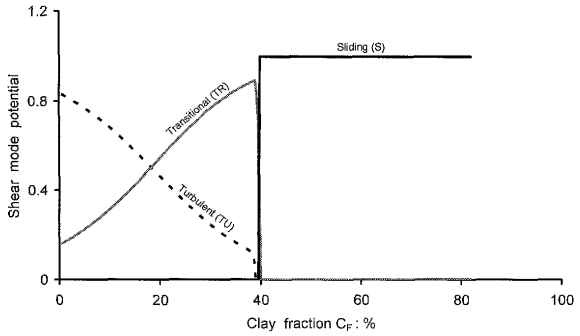

Fig. 12. Shear mode potential versus clay fraction, computed with artificial neural network analysis

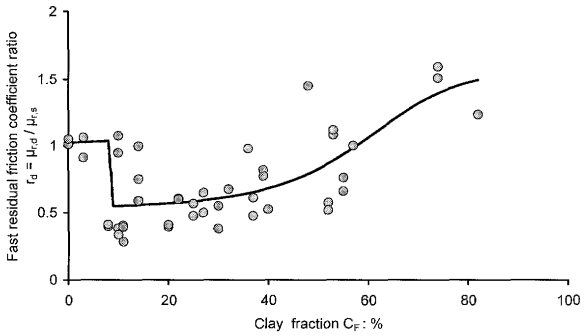

Fig. 13. Correlation of fast residual friction coefficient ratio (normalized with the slow residual friction coefficient $\mu_{r,s}$) with clay fraction: Comparison between experimental data and artificial neural network approximation: Data points taken from Tika et al., 1996 and Tika and Hutchinson, 1999

high for $20\% < C_F < 40\%$, and zero for $C_F > 40\%$. Finally, the possibility for sliding shear mode is zero for $C_F < 40\%$, and high for $C_F > 40\%$.

As mentioned in the introduction, the slow residual strength depends also on pore water chemistry and effective normal pressure. Unfortunately, these parameters have not been incorporated into the proposed methodology, due to insufficient information provided by scarce experimental data.

Several researchers have shown that the critical state friction angle φ_{cv} correlates with the plasticity index even if with substantial scatter. One such relationship (with large correlation error) has been proposed by Mitchell (1976):

$$\varphi_{cv} \approx \arcsin \lfloor 0.6 - 0.14 \log (I_p - 5) \rfloor \qquad (27)$$

In pre-existing shear surfaces with large clay fraction Eq. (27) overestimates φ_{cv}. Therefore, Eq. (27) is valid only for intact clays. A value of φ_{cv} close to the slow residual friction angle $\varphi_{r,s}$ is more realistic when reactivation of an old landslide is anticipated.

Parameters of Frictional Strain-Rate Behaviour

Multilayer perceptron neural networks were developed for the calibration of the viscous parameters of the model $\mu_{r,d}$, (Fig. 8(b)) and β (Fig. 8(c)). The latter, β, controls the sharpness of the transition from slow residual to fast residual state. The fast residual friction coefficient ratio $r_d = \mu_{r,d} / \mu_{r,s}$ is correlated solely with clay fraction C_F, whereas β is computed as a function of the effective normal pressure σ'_{n0}, clay activity A, and clay fraction C_F. The computed parameter $\mu_{r,d}$ is compared in Fig. 13, with experimental data of Tika et al. (1996) and Tika and Hutchinson (1999). Figure 14 demonstrates the agreement between measured (ring shear apparatus) and computed [Eq. (16)] fast residual friction coefficient ratio for a wide velocity range. Calibration of β was based on the neural network analysis. The expressions derived after training of the neural network are of the same form as Eqs. (25) and (26). The "weights" and "biases" of the network layers are given in Tables 3 and 4, for the fast residual friction coefficient ratio r_d, and the parameter β, respectively. The (min, max) values of the input parameters x_j are (0.177 MPa, 0.98 MPa), (0.4, 4) and (0, 80) for σ'_{n0}, A and C_F, respectively.

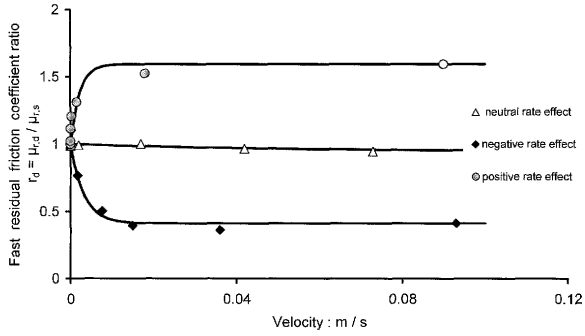

Fig. 14. Fast residual friction coefficient ratio (normalized with the friction coefficient μ_{cv} at critical void ratio) versus velocity. Comparison between measured in ring shear apparatus and computed behaviour, for $\beta = 310$, 20, and 452, corresponding to negative, neutral, and positive rate effect, respectively. The experimental points are from Tika and Hutchinson, 1999

In addition, a neural network was developed for soil classification according to the rate effect on residual strength. The output layer of the network consists of three output neurons, one corresponding to each class (neutral, negative, and positive rate effect), and target values of 1 for the correct class and 0, otherwise. The prediction of the neural network after the training, is plotted in Fig. 15. According to the results, the possibility for neutral rate effect is high for $C_F < 10\%$, low for $10\% < C_F < 20\%$, and zero for $C_F > 20\%$. The possibility for negative rate effect is zero for $C_F < 8\%$, high for $8\% < C_F < 40\%$, and low to medium for $C_F > 40\%$. Finally, the possibility for positive rate effect is zero for $C_F < 40\%$, and medium to high for $C_F > 40\%$.

Pore-Pressure-Temperature Coefficient

Little information is available for the pore-pressure-temperature coefficient, λ_m. Experimental data taken from Sultan (1997), Sulem et al. (2004), Baldi et al. (1991), Plum and Esrig (1967), and Laloui and Cekerevak (2003), identify the parameter λ_m as strongly dependent on overconsolidation stress ratio OCR. Typical values *of* α_c^{cp} (*see* Eq. (18)) for a normally consolidated clay

Table 3. Weights and biases for the fast residual friction coefficient ratio $r_d = \mu_{r,d}/\mu_{r,s}$

Hidden layer		Output layer	
$w1_{i,j}$	$b1_i$	$w2_i$	$b2$
−1.343	1.0445	−1.526	1.214
−197.872	−182.149	0.418	

Table 4. Weights and biases for parameter β

Hidden layer				Output layer	
$w1_{i,j}$			$b1_i$	$w2_i$	$b2$
−9.241	−7.408	−0.316	−5.201	−420.643	50.415
−9.76	−8.556	−1.796	−6.615	420.639	
6.601	−15.298	−3.435	−8.013	−256.493	
10.896	−22.158	0.202	−9.571	255.895	
7.848	−22.849	26.444	−21.492	−50.182	
68.732	56.857	7.434	102.301	−1.286	

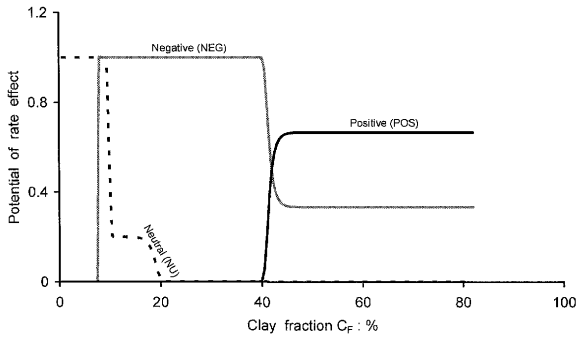

Fig. 15. Rate effect potential versus clay fraction, computed with artificial neural network analysis

(OCR = 1) are in the range of 1.5×10^{-4} °C^{-1} to 2.5×10^{-4} °C^{-1}. For slightly overconsolidated clays ($1 < \text{OCR} < 3$) the coefficient α_c^{ep} appears to be a decreasing function of OCR. Results from drained thermal loading of illite (Plum and Esrig, 1967) and of Boom clay specimens at constant isotropic stress (Baldi et al., 1991) indicate that the thermal volumetric strain vanishes with increasing OCR, reaching zero at OCR ≈ 2. Vardoulakis (2002) proposed an empirical correlation between the coefficient α_c^{ep} and OCR for overconsolidated clays, utilising experimental data from Sultan (1997):

$$\alpha_c^{ep} \approx -10^{-3} \exp\left(-\frac{\text{OCR}-1}{12}\right) \quad [°\text{C}^{-1}],$$

with

$$\text{OCR} = \frac{\sigma'_{n0}}{\sigma'_{n0} - p} \tag{28}$$

Notice in Eq. (28) that α_c^{ep} is not a constant but a function of the excess pore-water pressure p.

The elastic thermal coefficient α_c^{e} is estimated to be about 5 to 10 times smaller than the elastoplastic coefficient α_c^{ep} in normally consolidated and slightly overconsolidated clays. Hence, typical values for α_c^{e} of overconsolidated clays are in the range of 0.5×10^{-4} °C^{-1} to 1.5×10^{-4} °C^{-1}. As shown in Fig. 6, the elastic thermal coefficient α_c^{e} is a function of the overconsolidation stress ratio OCR, which in turn depends on the excess pore-water pressure p. However, due to insufficient information provided by scarce experimental data, it is considered as a constant in all the subsequent analysis.

Critical Temperature

Critical temperature, θ_{cr}, is the threshold for thermoplastic "*collapse*" of an overconsolidated clay. Exploiting experimental data from Sultan (1997), Vardoulakis (2002) proposed the following expression for θ_{cr} as a function of OCR:

$$\theta_{cr} \approx 40° + 60°\left[1 - \exp\left(-\frac{\text{OCR}-1}{10}\right)\right],$$

with

$$\text{OCR} = \frac{\sigma'_{n0}}{\sigma'_{n0} - p} \tag{29}$$

Compressibility Index

There is lack of information of any dependence of the recompression-swelling index, C_r, on temperature—hence our assumption is that C_r is independent of θ. Based on the modified Cam clay model, Wroth and Wood (1978) showed that C_r can be obtained as a function of the plasticity index:

$$C_r \approx \frac{I_p}{370} \tag{30}$$

Shear Band Thickness

The shear band thickness, d_b, is a critical modeling parameter, as it makes the strain-dependent Eqs. (17) and (21) of heat generated pore pressures compatible with the displacement-dependent Eqs. (2), (13), (15), and (16) of the viscoplastic frictional behaviour.

Morgenstern and Tschalenko (1967) documented the microscopic structure of shear bands in Kaolin specimens in direct shear tests, and also proposed that the shear-band thickness can be estimated as a function of the particle size d_{50}, according to;

$$d_b \approx 200 d_{50} \tag{31}$$

As a matter of fact, Eq. (31) is considered to give a lower bound estimate of d_b. Results from back analysis of the well-documented Vaiont landslide, indicated that values of d_b in the range of 0.1 m to 0.2 m are quite reasonable (Vardoulakis, 2000). Such high values are justified if we assume that the active shear band thickness increases in the course of sliding.

NUMERICAL FORMULATION OF THE SHEAR BAND MODEL

The system of differential Eqs. (1), (2), (13), (17) and (21) describes mathematically the deformation of the

Table 5. List of materials and model parameters used in the analysis of shear band dynamic deformation

Parameters	Case study				
	A1	A2	B1	B2	C
Clay mineral	Kaolinite	Kaolinite	Montmorillonite	Montmorillonite	Illite
Shear mode	TR	S	TR	S	TR
Rabe effect	NEG	POS	NEG	POS	NEG
C_F (%)	30	70	30	70	30
A	0.4	0.4	4	4	0.9
ϕ_{cv} (deg)	28	24	18	15	26
$\phi_{r,s}$ (deg)	25	13	10	5	16
$\phi_{r,d}$ (deg)	16	17	6	6.5	10
C_r	0.032	0.075	0.32	0.75	0.073
e_0	0.22				
σ'_{n0} (MPa)	1, (0.2, 0.5, 2, 5)*				
OCR	1.5				
ν	0.2				
θ_0 (°C)	10				
θ_{evp} (°C)	180, (124, 154, 210, 256)*				
α_c^e (°C^{-1})	$7.4\ 10^{-5}$				
u_{cv} (m)	0.01				
d_b (m)	0.0015, (0.01, 0.05, 0.1)*				
k	0.01				
λ	4000				
n	1				
b	0.5				
u_y (m)	0.001				

*Only for case C

shear band. An explicit finite-difference algorithm has been developed for the solution of this system. The algorithm was incorporated into a computer code, DSC-LANDSLIDE (developed under the framework of the research project LESSLOSS, 2005), for the analysis of earthquake triggering and evolution of catastrophic landslides.

SHEAR BAND DYNAMIC DEFORMATION: ANALYSIS AND DISCUSSION

The developed model is utilised to study the dynamic deformation of a shear band in clay-rich material subjected to a constant velocity of $v=0.1$ m/s. As already mentioned in the introduction, at such high velocity the fast residual strength will be fully mobilized. Four cases are considered of varying clay mineral and clay fraction inside the shear band:

- kaolinite with $C_F=30\%$ and $C_F=70\%$,
- montmorillonite with $C_F=30\%$ and $C_F=70\%$.

The model and material parameters used in each case are summarised in Table 5. Their calibration was based on the aforementioned neural network methodology. It is stated however, that there are no available experimental data to support the validity of the analysis.

The computed evolution with the progress of sliding displacement of: (a) the normalized shear stress ratio, (b) the apparent friction coefficient ratio, (c) the temperature and critical temperature, and (d) the excess pore-water pressure ratio are plotted in Figs. 16–17. The following observations are worthy of notice in these figures:

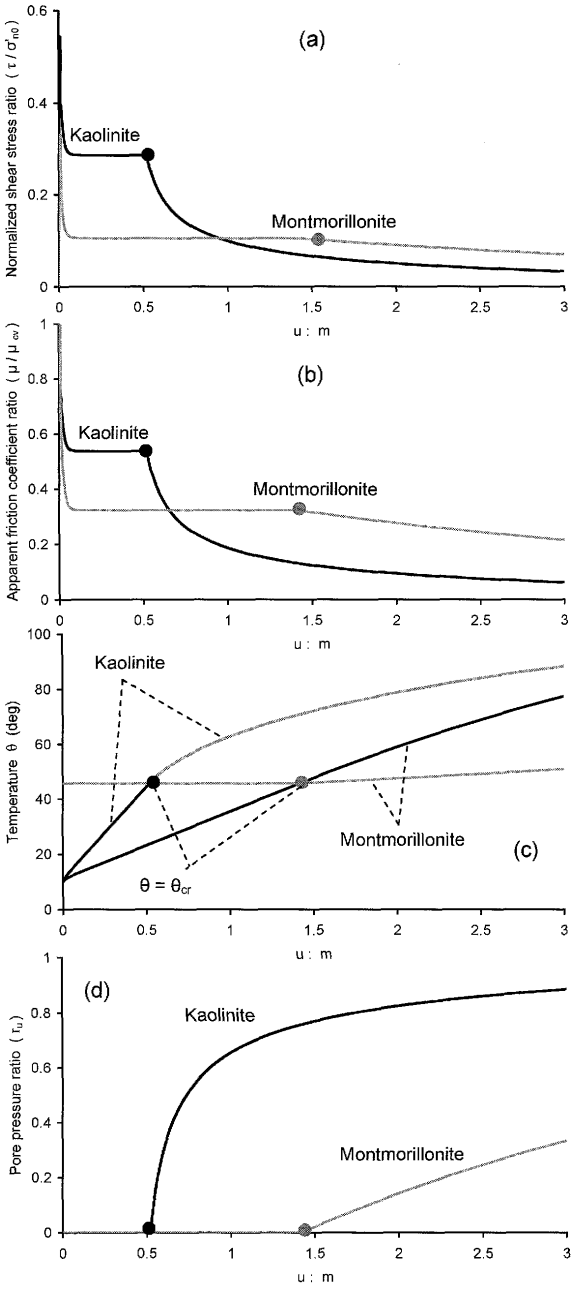

Fig. 16. Evolution with displacement of: (a) the normalized shear stress ratio τ/σ'_{n0}, (b) the apparent friction coefficient ratio μ/μ_{cv}, (c) the temperature θ (black line) and the critical temperature θ_{cr} (gray line) and (d) the developing excess pore pressure ratio r_u ($=p/\sigma'_{n0}$), for cases A1 (Kaolinite with $C_F=30\%$) and B1 (Montmorillonite with $C_F=30\%$): Both soils exhibit transitional shear mode (TR) and negative rate effect (NEG)

(a) In all cases, montmorillonite exhibited the slower reduction in shear resistance. Although the peak strength of montmorillonite is about 1.5 times smaller than that of kaolinite, its mobilized shear resistance after 3 m of sliding is approximately two times larger than that of kaolinite when negative rate effect is involved and three times larger when positive rate effect is considered. The "ductile" shear behaviour of montmorillonite, or the (more) "brittle" behaviour of kaolinite, is attributed to the following reasons:

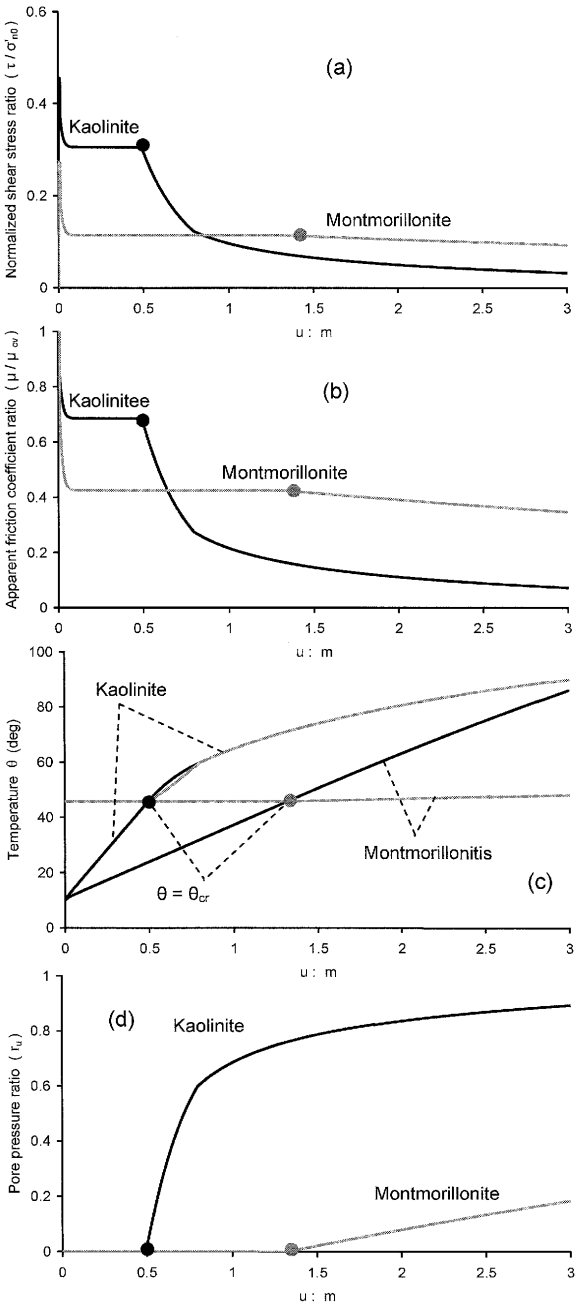

Fig. 17. Evolution with displacement of: (a) the normalized shear stress ratio τ/σ'_{n0}, (b) apparent friction coefficient ratio μ/μ_{cv}, (c) the temperature θ (black line) and the critical temperature θ_{cr} (gray line) and (d) the developing excess pore pressure ratio r_u ($=p/\sigma'_{n0}$), for cases A2 (Kaolinite with $C_F=70\%$) and B2 (Montmorillonite with $C_F=70\%$): Both soils exhibit sliding shear mode (S) and positive rate effect (POS)

- The small residual strength of montmorillonite, mobilized at the very early stage of sliding, results in a significant reduction of frictional heating which in turn slows down the excess pore-water pressure generation, and thus the shear strength reduction.
- The larger compressibility of montmorillonite, the index of which (C_r) is an order of magnitude larger than that of kaolinite, results in a smaller pore-pressure-temperature coefficient, leading to a further de-acceleration of the shear strength softening.

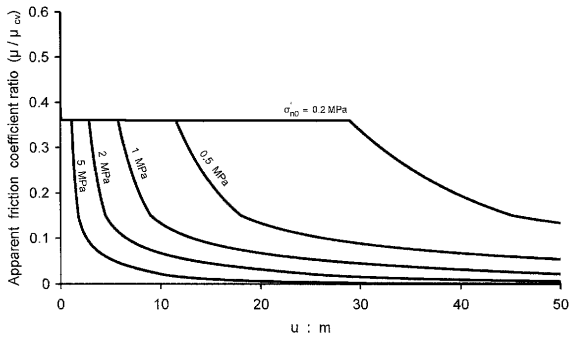

Fig. 18. Evolution of apparent friction coefficient ratio μ/μ_{cv} with displacement for values of initial effective normal pressure $\sigma'_{n0}=$ 0.2, 0.5, 1, 2, and 5 MPa (Case C: Illite with $C_F=30\%$)

(b) The displacement u_{cr} at which thermo-poro-mechanical softening is initiated, is practically unaffected by the rate effect on residual strength. This critical, for the landslide evolution, displacement is computed to be approximately 0.5 m in kaolinite and 1.4 m in montmorillonite.

(c) The influence of rate effect (positive or negative) on the evolution of shear resistance during the thermo-poro-mechanical softening phase, is negligible in the case of kaolinite, but appreciable for montmorillonite.

Parametric analysis were also carried out to investigate the influence of the initial effective normal pressure σ'_{n0} and the shear band thickness d_b on the evolution of a catastrophic landslide. The case considered is that of a shear band rich in illite with clay fraction $C_F=30\%$, moving at a constant velocity of $v=0.1$ m/s. The model and material parameters used in the analysis (case C) are presented in Table 5.

Figure 18 illustrates the evolution of the apparent friction coefficient ratio with sliding, at four levels of initial effective pressure σ'_{n0} ($=0.2$ MPa, 0.5 MPa, 1 MPa, 2 MPa, and 5 MPa). It appears that the displacement required for temperature "explosion" decreases with increasing σ'_{n0}. In other words, the shear behaviour becomes more brittle at higher values of σ'_{n0}, increasing the potential of a catastrophic landslide. It is also mentioned that the evaporation limit θ_{evp} was not reached in any of the cases. Figure 19 elucidates the displacement required for thermal "explosion" as a function of the shear band thickness d_b, for selected values of initial effective normal pressure σ'_{n0}. It is demonstrated that at low levels of σ'_{n0} ($=0.2$ MPa), the mechanism of thermo-poro-mechanical softening would only be activated if d_b is of the order of few millimeters. At greater values of σ'_{n0} (in excess of 2 MPa), however, thermal "explosion" and heat generated pore pressures may rise even for the extreme case of $d_b=0.1$ m. It is noted, that Vardoulakis (2002) estimated an average value of $\sigma'_{n0}=2.38$ MPa as representative for the Vaiont landslide.

The capability of the model is further demonstrated through analysis of the shear band response under cyclic

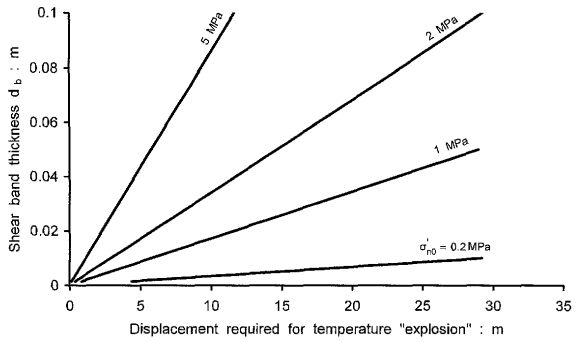

Fig. 19. Curves of shear band thickness d_b versus displacement required for temperature "explosion" (initiation of pore-water pressure rise) for values of initial effective normal pressure σ'_{n0} = 0.2, 1, 2, and 5 MPa (Case C: Illite with C_F = 30%)

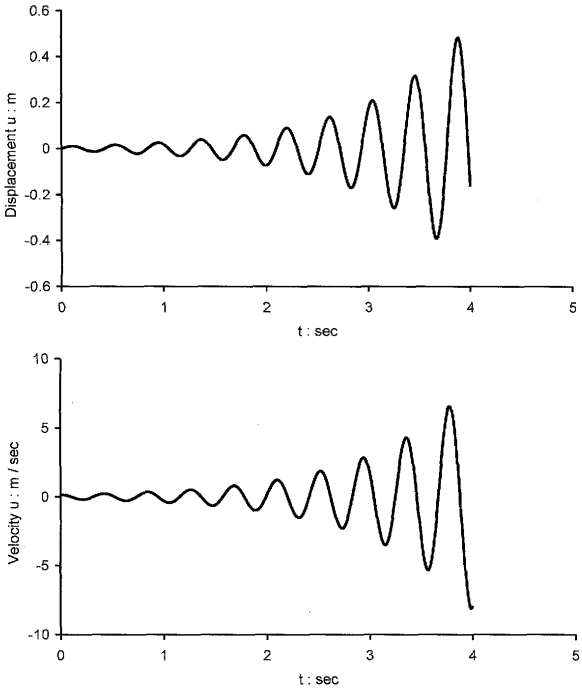

Fig. 20. Example of the effects of oscillatory loading: imposed displacement and velocity time histories (Case C: Illite with C_F = 30%, d_b = 0.0015 m, σ'_{n0} = 1 MPa)

loading. The shear band is subjected to a displacement time history of increasing amplitude with time. The imposed displacement and resulted velocity time histories are portrayed in Fig. 20. The material and model parameters used in the analysis are those of case C (Table 5). Unfortunately, according to the authors' knowledge there are no relevant experimental results in the literature to compare with the prediction of the model.

Figure 21 portrays the shear stress ratio-displacement hysteretic loops. It is observed that the shear strength is progressively degrading with cyclic loading reaching an ultimate level, which is the fast residual strength. The corresponding evolution of the friction coefficient ratio is depicted in Fig. 22. Notice that, the shear strength is not recovering at any time during loading, in agreement with laboratory results showing that once preferred particle

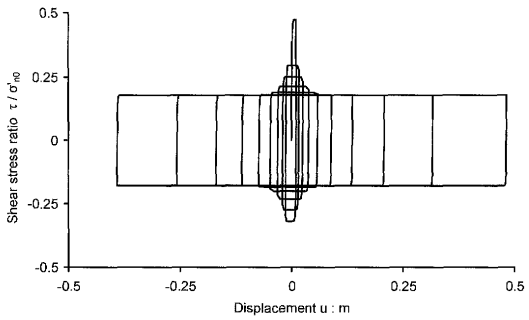

Fig. 21. Example of the effects of oscillatory loading: shear stress ratio versus displacement hysteresis loops (Case C: Illite with C_F = 30%, d_b = 0.0015 m, σ'_{n0} = 1 MPa)

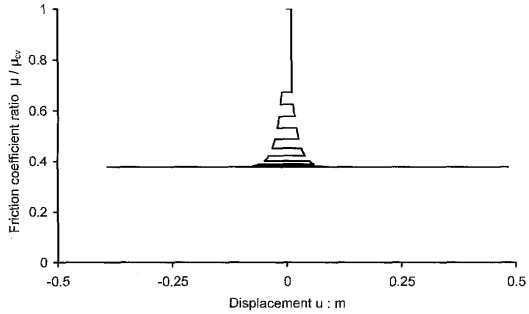

Fig. 22. Example of the effects of oscillatory loading: evolution of the friction coefficient ratio with displacement (Case C: Illite with C_F = 30%, d_b = 0.0015 m, σ'_{n0} = 1 MPa)

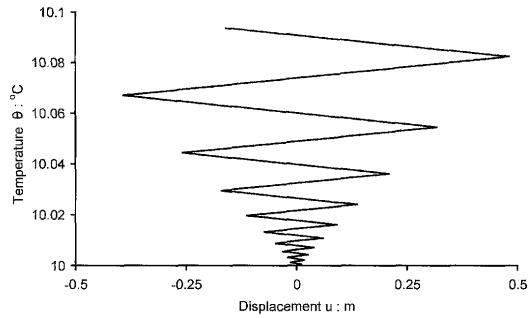

Fig. 23. Example of the effects of oscillatory loading: evolution of temperature with displacement (Case C: Illite with C_F = 30%, d_b = 0.0015 m, σ'_{n0} = 1 MPa)

orientation has occurred, the shear resistance becomes insensitive to loading history (Lupini et al., 1981). Figure 23 shows that the temperature rise is practically negligible, meaning that heat generated pore pressures in this case of cyclic loading do not develop even at velocities as large as 8 m/s. Such a value for velocity is far larger than those developed in a strong seismic motion (which only rarely reach 1.5 m/s), revealing indirectly that thermo-poro-mechanical softening is associated only with the high speeds developing in the course of sliding, driven by gravity forces; even if the triggering of such sliding was provided by the seismic shaking—a phenomenon reminiscent of liquefaction-induced flow of slopes: the seismic shaking strains the material and high

excess pore-water pressures develop leading to liquefaction. But only if the residual strength of the liquefied soil is overwhelmed by the gravity-induced shear stresses will "flow" and large deformation take place.

CONCLUSION

A constitutive model for rapid deformation of a clay-rich shear zone has been developed utilizing the concept of frictional softening due to heat generated excess pore-water pressures. The model is incorporated into a novel algorithm named DSC-Landslide for the analysis of earthquake-induced catastrophic landslides. A methodology is developed, based on multi-layered artificial neural networks, for the calibration of the model parameters against published laboratory results. A sensitivity analysis is conducted for the influence of key model parameters (initial effective normal stress and shear band thickness) on the pore-water pressure rise due to increase in temperature. The capability of the model is demonstrated in a numerical study leading to some interesting conjectures (which, however, are for the moment without experimental verification):

(a) Clay activity has a decisive role in the evolution of the landslide: larger activity (e.g. montmorillonite) leads to less rapid slide.

(b) The influence of the rate effect on residual strength (positive or negative) on the landslide evolution increases with increasing clay activity.

(c) The initial effective normal stress σ'_{n0} and shear band thickness d_b greatly affect the evolution of the landslide, with greater values of σ'_{n0} and smaller values of d_b, respectively, resulting in more brittle and accelerated slides.

(d) Thermo-poro-mechanical softening is associated only with sliding driven by gravity forces and not with earthquake-induced loading.

Application of the proposed model to real case studies (e.g. the Jiufengershan, 1999 landslide triggered by the Chi-Chi Taiwan earthquake (Chang et al., 2005)) would strengthen the validity of the aforementioned conclusions.

ACKNOWLEDGMENTS

This paper is a partial result of the Project PYTHAGORAS I/EPEAEK II (Operational Programme for Educational and Vocational Training II) [Title of the individual program: Mathematical and experimental modeling of the generation, evolution and termination mechanisms of catastrophic landslides]. This Project is co-funded by the European Social Fund (75%) of the European Union and by National Resources (25%) of the Greek Ministry of Education.

REFERENCES

1) Anson, R. W. W. and Hawkins, A. B. (1998): The effect of calcium ions in pore water on the residual shear strength of kaolinite and sodium montmorillonite, *Geotechnique*, **48**(6), 787–800.
2) Baldi, T., Hueckel, A., Peano and Pellegrini, R. (1991): Developments in modeling of thermo-hydro-geomechanical behaviour of Boom clay and clay-based buffer materials, *Report EUR 13365*, Commission of the European Communities, Nuclear Science and Technology.
3) Bishop, A. W., Green, G. E., Garga, V. K., Andresen, A. and Brown, J. D. (1971): A new ring shear apparatus and its application to the measurement of residual strength, *Geotechnique*, **21**(4), 273–328.
4) Bouc, R. (1971): Modele mathematique d' hysteresis, *Acustica*, **21**, 16–25.
5) Bromhead, E. N. and Curtis, R. D. (1983): A comparison of alternative methods of measuring the residual strength of London Clay, *Ground Engineering*, **16**, 39–41.
6) Campanella, R. G. and Michell, J. K. (1968): Influence of temperature variations on soil behavior, *J. Soil Mech. Found.*, ASCE, **94**, 709–734.
7) Chang, K. J., Taboada, A., Lin, M. L. and Chen, R. F. (2005): Analysis of landsliding by earthquake shaking using a block-on-slope thermo-mechanical model: Example of Jiufengershan landslide, central Taiwan, *Engineering Geology*, **80**, 151–163.
8) Despax, D. (1976): Influence de la temperature sur les proprietes des argiles saturees. *Doctoral Thesis*, Ecole Centrale de Paris.
9) Drescher, A., Vardoulakis, I. and Han, C. (1990): A biaxial apparatus for testing soils, *Geotech. Test. J.*, GTJODJ **13**, 226–234.
10) Fodil, A., Aloulou, W. and Hicher, P. Y. (1997): Viscoplastic behaviour of soft clay, *Geotechnique*, **47**(3), 581–591.
11) Gerolymos, N. and Gazetas, G. (2005): Constitutive model for 1-D cyclic soil behaviour applied to seismic analysis of layered deposits, *Soils and Foundations*, **45**(3).
12) Habid, P. (1967): Sur un mode de glissement des massifs rocheux, *C. R. Hebd Seanc*, Academy of Science, Paris, **264**, 151–153.
13) Habid, P. (1976): Production of gaseous pore pressure during rock slides, *Rock Mechanics*, **7**, 193–197.
14) Hicher, P. Y. (1974): Etude des proprietes mecaniques des argiles a l' aide d' essays triaxiaux, influence de la vitesse et de la temperature, *Report Soil Mech. Labo.*, Ecole Central, de Paris.
15) Hueckel, T. and Baldi, G. (1990): Thermo-plasticity of saturated soils and shales: constitutive equations, *J. Geotech. Engrg.*, **116**, 1765–1777.
16) Hueckel, T., Pellegrini, R. and Del Olmo, C. (1998): A constitutive study of thermo-elasto-plasticity of deep carbonatic clays, *Int. J. Num. Anal. Meth. Geomech.*, **22**, 549–574.
17) Laloui, L. and Modaressi, H. (2002): Modelling of the thermo-hydro-plastic behaviour of clays, *Hydromechanical and Thermo-hydromechanical Behaviour of Deeo Argillaceous Rock*, (eds. by Hoteit et al.), Swets & Zeitlinger, Lisse, 161–173.
18) Laloui, L. and Cekerevac, C. (2003): Thermo-plasticity of clays: An isotropic yield mechanism, *Comput. Geotech.*, **30**, 649–660.
19) LESSLOSS Integrated R&D Project of the EC (2005): Risk Mitigation of Earthquakes and Landslides, EU sixth Framework Program, Contract number: GOCE-CT-2003-505448, http://www.lessloss.org.
20) Lupini, J. F., Skinner, A. E. and Vaughan, P. R. (1981): The drained residual strength of cohesive soils, *Geotechnique*, **31**(2), 181–213.
21) MATLAB (2000): *The Language of Technical Computing*, Copyright 1984–2000 The MathWorks, Inc.
22) Mench, V. (1966): Mechanics of landslides with noncircular slip surfaces with special reference to the Vaiont slide, *Geotechnique*, **16**, 330–337.
23) Mitchell, J. K. (1976): *Fundamentals of Soil Behaviour*, John Wiley and Sons, New York, 422.
24) Modaressi, H., Faccioli, E., Aubry, D. and Noret, C. (1995): Numerical modelling approaches for the analysis of earthquake triggered landslides, *Proc. 3rd Int. Conf. Recent Advances in Geotech. Earthquake Engrg, Soil Dynam.*, St. Louis, Missouri, **II** (INVLE.03), 833–843.
25) Modaressi, H. and Laloui, L. (1997): A thermo-viscoplastic

constitutive model for clays, *Int. J. Num. Anal. Meth. Geomech.*, **21**, 313–335.
26) Moore, R. (1991): The chemical and mineralogical controls upon the residual strength of pure and natural clays, *Geotechnique*, **41**(1), 35–47.
27) Muller, L. (1964): The rock slide in the Vaiont Valley, *Rock Mechanics Engineering Geology*, **2**, 148–212.
28) Muller, L. (1968): New considerations on the Vaiont slide, *Rock Mechanics Engineering Geology*, **6**, 1–91.
29) Nova, R. (1986): Soil models as a basis for modeling the behaviour of geophysical materials, *Acta Mechanical*, **64**, 31–44.
30) Otsuki, K. (1978): On the relationship between the width of the shear zone and the displacement along the fault, *J. Geolog. Soc. Jpn.*, **84**, 661–669.
31) Picard, J. (1994): Ecroisage thermique des argiles saturées: application au stockage des déchets radioactifs, *Thés de Doctorat*, l'Ecole Nationale des Ponds et Chaussées, Paris.
32) Plum, R. L. and Esrig, M. I. (1967): Some temperature effects on soil compressibility and pore water pressure, *Highway Res. Board* (Sp. Rpt), **103**, 231–242.
33) Skempton, A. W. (1985): Residual strength of clays in landslides, folded strata and the laboratory, *Geotechnique*, **35**(1), 3–18.
34) Sulem, J., Vardoulakis, I., Ouffroukh, H. and Perdikatsis, V. (2004): Thermo-poro-mechanical properties of the aigion fault clayey gouge-application to the analysis of shear heating and fluid pressurization, *Soils and Foundations*, **45**(2), 97–108.
35) Sultan, N. (1997): Etude du comportement thermo-mechanique de l'argile de Boom: experiences et modelisation, *These de Doctorat*, ENPC, CERMES, Paris.
36) Tika, T. E., Vaughan, P. R. and Lemos, L. J. (1996): Fast shearing of pre-existing shear zones in soil, *Geotechnique*, **46**(2), 197–233.
37) Tika, Th.E. and Hutchinson, J. N. (1999): Ring shear tests on soil from the Vaiont landslide slip surface, *Geotechnique*, **49**(1), 59–74.
38) Vardoulakis, I. (2000): Catastrophic landslides due to frictional heating of the failure plane, *Mechanics of Cohesive-Frictional Materials*, **5**, 443–467.
39) Vardoulakis, I. (2002): Dynamic thermo-poro-mechanical analysis of catastrophic landslides, *Geotechnique*, **52**(3), 157–171.
40) Vardoulakis, I. (2002): Steady shear and thermal run-away in clayey gouges, *Int. J. Solids and Structures*, **39**, 3831–3844.
41) Voight, B. and Faust, C. (1982): Frictional heat and strength loss in some rapid landslides, *Geotechnique*, **32**(1), 43–54.
42) Waterson, J. (1986): Fault dimensions, displacement and growth, *Pageophysics*, **124**, 365–373.
43) Wen, Y.-K. (1976): Method for random vibration of hysteretic systems, *J. Engrg. Mech., ASCE*, **102**, 249–263.
44) Wroth, C. P. and Wood, D. M. (1978): The correlation of index properties with some basic engineering properties of soils, *Can. Geotech. J.*, **15**(2), 137–145.